Focusing of high-wave-vector magnons

J. J. Bible and R. E. Camley
Physics Department, University of Colorado at Colorado Springs, Colorado Springs, Colorado 80918, USA
(Received 21 December 2016; published 8 June 2017)

The focusing of spin waves in magnetic materials has a number of important advantages for directing energy and thus information. In contrast to earlier works, we theoretically calculate the focusing of short-wavelength spin waves. We show that strong focusing of large wave-vector spin waves naturally occurs about halfway out in the Brillouin zone with no need for a magnetocrystalline anisotropy, dipolar effects, or an external magnetic field. The fact that the wavelength is on the order of the lattice constant leads to a form of lattice-induced anisotropy in the wave propagation. We also explore the tunability that is achieved by the application of both an external field and a uniaxial anisotropy. In this case there is a rotation of the focusing pattern. The rotation angle can be changed by varying the field strength, demonstrating tunability.

DOI: 10.1103/PhysRevB.95.224412

I. INTRODUCTION

In an isotropic material the energy from a point source will spread out uniformly in all directions. In contrast in anisotropic materials the phase and group velocities are not parallel and the energy from a point source may be preferentially focused into specific directions. When focused beams are especially narrow, these directions are known as caustic (for burning) beams. (Technically caustics occur when the curvature of the constant frequency curves in k space is zero.) Even when reflected from a boundary, this energy follows very specific directions and, surprisingly, the incident and reflected angles are not equal.

There is considerable literature on the focusing of both bulk and surface phonons in elastic solids. For example, phonon focusing can be created by exciting a crystal with a pulsed laser [1,2] or by heat pulses [3,4]. Depending on the elastic anisotropy, the frequency, and the dispersion relation, it is possible to precisely focus energy in limited and specific directions. There are numerous examples of this in both theory [5] and experiments [6,7] with excellent agreement.

Phonon systems are limited in practical applications because the focusing is not tunable. Recently, focusing of magnetic spin waves has been observed [8] using Brillouin light scattering (BLS) to examine the propagation of a spin wave from a source on the surface of yttrium iron garnet (YIG). The focusing of magnons, or spin waves in magnetic systems, has a number of important advantages. As an example, focusing in a magnetic system is tunable by varying both the strength and direction of an applied magnetic field [9].

Until now, only long-wavelength spin waves have been examined [8–15]. In this earlier work, the magnetic dispersion relation was anisotropic because of dipolar interactions and an external magnetic field. In addition to the anisotropic magnon dispersion, observation of magnetic focusing generally requires the creation of spin waves in a localized region. Experimentally this can be done by localized microwave currents that create oscillating magnetic fields. Other methods can also be used. For example, if we consider a magnetic antidot in a continuous YIG lattice there is a nonuniform internal magnetic field in the vicinity of the isolated antidot. Exposing the sample to a harmonic microwave field, one can excite only the regions near the antidot, because the resonance field there is different from the rest of the structure. The antidot will react as a point source and caustics can result [8,10].

Our work, in contrast, extends the theory by discussing the focusing that occurs naturally in spin waves of shorter wavelengths, without a requirement for an external magnetic field, dipolar effects, or any magnetocrstalline anisotropy. We find a number of interesting features

(1) Strong focusing, i.e., caustics, occurs about halfway out in the first Brillouin zone, where the wavelengths are much shorter than those examined previously.

(2) An effective anisotropy results from the lattice structure itself rather than because of dipolar effects or magnetocrystalline anisotropy [15].

(3) The appearance of focusing and the focusing pattern can be significantly changed by next nearest neighbor exchange interactions.

In this paper, we examine multiple scenarios. Nearest and next nearest neighbor exchange interactions are explored, with both an external field and/or anisotropy. We present a short theoretical derivation for the dispersion relations of various cases. The magnetic configurations and dispersion relations are derived from the Landau-Lifshitz equations, and the focusing patterns are obtained from constant frequency curves (slowness surfaces) in wave-vector space.

We analyze the focusing patterns and their amplitudes at various frequencies. With both a uniaxial anisotropy and an external field, we find that the slowness surfaces and focusing patterns can be rotated. This rotation provides an important example of external field induced system tunability. The existence of focusing along with the ability to control spin wave direction allows the development of signal processing systems [16]. This could be important for spintronics, where the transfer of angular momentum is a key factor. The ability to focus energy strongly in specific directions implies the ability to focus angular momentum transport.

II. THEORY

We begin by obtaining the dispersion relation for various physical cases. These dispersion relations are subsequently used to obtain the focusing patterns.

We examine the following cases.

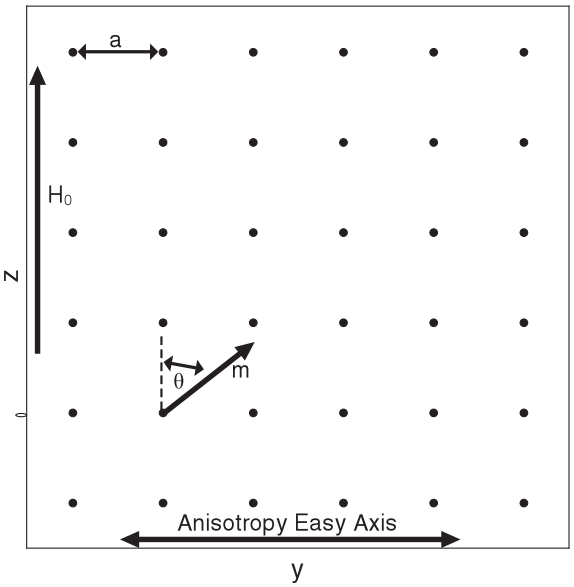

FIG. 1. Diagram of the physical lattice in the zy plane. The spacing between lattice points is a. When present, there is a magnetic field along $\hat{z}$ and the y axis is an easy axis for uniaxial anisotropy. Notice the equilibrium angle θ between the field and the magnetic moments.

(1) A two dimensional square lattice with nearest and next nearest exchange interactions and with an external field or a uniaxial anisotropy in the plane of the lattice.

(2) A two dimensional square lattice with nearest neighbor exchange interactions, an external magnetic field in the plane of the lattice, and a uniaxial anisotropy with an easy axis perpendicular to the external field, also in the plane of the lattice.

The geometry is illustrated in Fig. 1. In the absence of an external field or anisotropy, we assume the spins lie in the yz plane and are directed along the z axis. When both anisotropy and a field are present the magnetic moments in equilibrium will make an angle θ with the z axis.

We find equations of motion for the magnetic moment at a site (i,j), denoted by $\mathbf{m}(i,j) = g\mu_b \mathbf{S}(i,j)$, using the effective field produced by the exchange,

$$\dot{\mathbf{m}}(i,j) = \gamma(\mathbf{m}(i,j) \times \mathbf{H}_{\text{eff}}). \tag{1}$$

The effective field is found from the exchange interaction,

$$\mathbf{H}_{\text{eff}}(i,j) = \underbrace{J_1 \sum_{\delta_1,\delta_2} \mathbf{m}(i+\delta_1, j+\delta_2)}_{\text{nearest neighbor}} + \underbrace{J_2 \sum_{\delta_1,\delta_2} \mathbf{m}(i+\delta_1, j+\delta_2)}_{\text{next nearest neighbor}}, \tag{2}$$

where J_1 is the nearest neighbor exchange constant and J_2 is the next nearest neighbor exchange constant. We sum over integers δ_1 and δ_2 to examine all of the nearest neighbor and next nearest neighbor sites. We impose conditions on $\mathbf{m}$ in order to linearize our equations of motion. We assume that in the z direction $m_z \approx m$ and that m_x and m_y are small so second order terms can be ignored. We also assume a wavelike solution propagating in the yz plane:

$$\mathbf{m}(i,j) = \mathbf{m}_0 e^{ik_z ai} e^{ik_y aj} e^{-i\omega t}. \tag{3}$$

We obtain the dispersion relation,

$$\omega = 2\gamma J_1 m(2 - \cos(ak_z) - \cos(ak_y)) + 4\gamma J_2 m(1 - \cos(ak_z)\cos(ak_y)). \tag{4}$$

For the situation where $J_2 = 0$ this simplifies to the well known result for nearest neighbors [17],

$$\omega = \gamma J m(4 - 2\cos(ak_z) - 2\cos(ak_y)). \tag{5}$$

If we add either an external magnetic field H_0 or a uniaxial anisotropy, strength K, both in the plane of the lattice, the results are not significantly different. The dispersion relation, using nearest neighbor exchange, is then given by

$$\omega_{\text{anisotropy}} = 4\gamma J m + \gamma \tfrac{K}{m} - 2\gamma J m(\cos(k_z a) + \cos(k_y a))$$

or

$$\omega_{\text{field}} = 4\gamma J m + \gamma H_0 - 2\gamma J m(\cos(k_z a) + \cos(k_y a)). \tag{6}$$

One can see that the frequency curves will be changed by a constant. This will therefore not change the focusing patterns; however, it will change the frequencies where focusing occurs.

We next consider the situation with uniaxial anisotropy and an external field, both in the plane of the lattice and perpendicular to each other. Assuming the H_0 field is in the $\hat{z}$ direction and the y axis is the anisotropic easy axis, there will be some angle θ from the z axis between the two fields where the magnetization is at equilibrium. K is the anisotropy constant and is assumed to be negative. We find this angle by minimizing the total energy:

$$E(i,j) = \frac{K}{2}\sin^2\theta - m(i,j)H(i,j)\cos\theta - J\sum_{\delta_1,\delta_2} \mathbf{m}(i,j)\cdot\mathbf{m}(i+\delta_1, j+\delta_2). \tag{7}$$

Minimizing this gives the angle of the magnetic moment at each site:

$$\theta = \arccos\left(-\frac{mH_0}{K}\right). \tag{8}$$

We rotate about the x axis counterclockwise by θ and obtain a new reference frame, the primed frame, with z' along the equilibrium direction. In order to linearize our equation, we assume that $m_{z'}(i,j) \approx m$. Furthermore, $\mathbf{m}_1 \cdot \mathbf{m}_2$ is invariant under rotation. From $E(i,j)$ we obtain the effective fields in the new coordinate system:

$$(H_{\text{eff}})_{x'}(i,j) = -J\sum_{\delta_1,\delta_2} m_{x'}(i+\delta_1, j+\delta_2), \tag{9}$$

$$(H_{\text{eff}})_{y'}(i,j) = -J\sum_{\delta_1,\delta_2} m_{y'}(i+\delta_1, j+\delta_2) - \frac{K}{m^2}\cos^2\theta m_{y'}(i,j) + \frac{K}{m}\sin\theta\cos\theta + H_0\sin\theta, \tag{10}$$

$$(H_{\text{eff}})_{z'}(i,j) = -4Jm - \frac{K}{m}\sin^2\theta + H_0\cos\theta + \frac{K}{m^2}\sin\theta\cos\theta m_{y'}(i,j). \tag{11}$$

We find the equations of motions in the primed frame from the effective fields using $\dot{\mathbf{m}} = \gamma(\mathbf{m} \times \mathbf{H}_{\text{eff}})$. From our previous solution for θ [Eq. (8)] we have the condition $H_0 \sin\theta = \frac{K}{m} \sin\theta \cos\theta$. This shows that $\dot{m}_{z'} = 0$. The equations for the transverse components become

$$\dot{m}_{x'}(i,j) = \left(-4\gamma Jm + \frac{\gamma K}{m}\cos(2\theta) + \gamma H_0 \cos\theta\right) \cdot m_{y'}(i,j) + \gamma Jm \sum_{\delta_1,\delta_2} m_{y'}(i+\delta_1, j+\delta_2), \tag{12}$$

$$\dot{m}_{y'}(i,j) = \left(4\gamma Jm + \frac{\gamma K}{m}\sin^2\theta - \gamma H_0 \cos\theta\right) \cdot m_{x'}(i,j) - \gamma Jm \sum_{\delta_1,\delta_2} m_{x'}(i+\delta_1, j+\delta_2). \tag{13}$$

Assuming a wavelike solution for $m_{x'}$ and $m_{y'}$ we obtain the dispersion relation for the case where the external field is perpendicular to an anisotropy and both are in the plane of the lattice, with exchange interactions:

$$\omega^2 = -\Big(\gamma Jm\big(4 - 2\cos(k_z a) - 2\cos(k_y a)\big) - \frac{\gamma K}{m}\cos(2\theta) - \gamma H_0 \cos\theta\Big)\Big(\gamma Jm(4 - 2\cos(k_z a) - 2\cos(k_y a)) + \frac{\gamma K}{m}\sin^2\theta - \gamma H_0 \cos\theta\Big). \tag{14}$$

We find the focusing pattern from the slowness surface. Because the group velocity is given by $\mathbf{v}_{\text{group}} = \nabla_{\mathbf{k}}(\omega)$ the direction of energy flow is normal to the constant frequency curves. From earlier work [5], it is known that the amplitude of the focusing is proportional to $\frac{1}{\sqrt{\text{curvature}}}$ of the slowness surface. We note that these analytic results were found for the far-field region. This approximation for the amplitude of the focusing is obviously only valid where the curvature is nonzero. As shown in [5] the focused energy is still finite even when the curvature is zero. In order to find the curvature, the

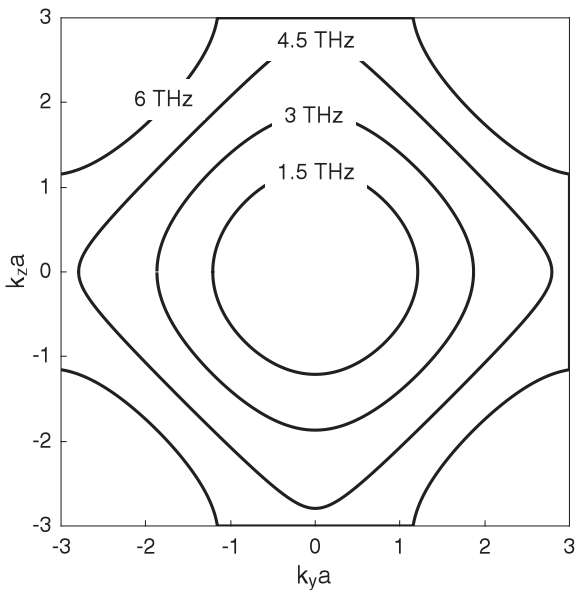

FIG. 2. Contours of constant frequency (slowness surfaces) for nearest neighbor interactions only. Focusing will occur near 4.5 THz.

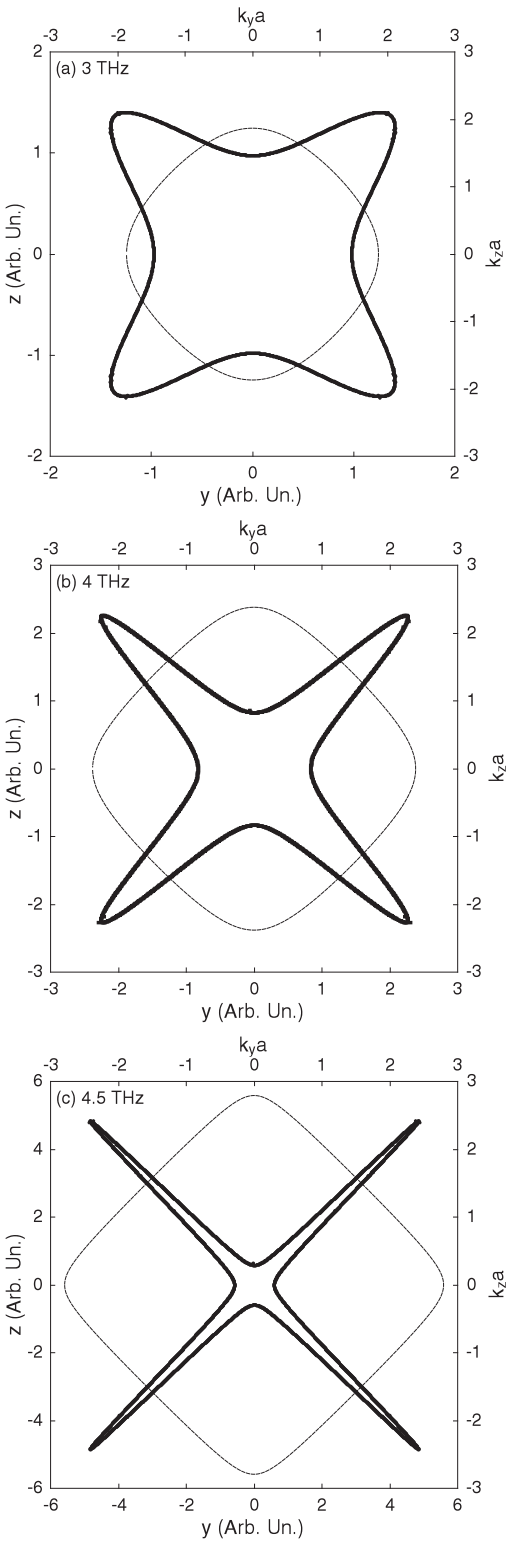

FIG. 3. Focusing patterns (dark curves using bottom and left axes) and associated slowness surfaces (light curves using top and right axes) at (a) $f = 3$ THz, (b) $f = 4$ THz, and (c) $f = 4.5$ THz for nearest neighbor interactions only. The pattern in (a) is hardly focused, while the pattern in (c) shows strong focusing. Notice the change in the axes from (a) to (c).

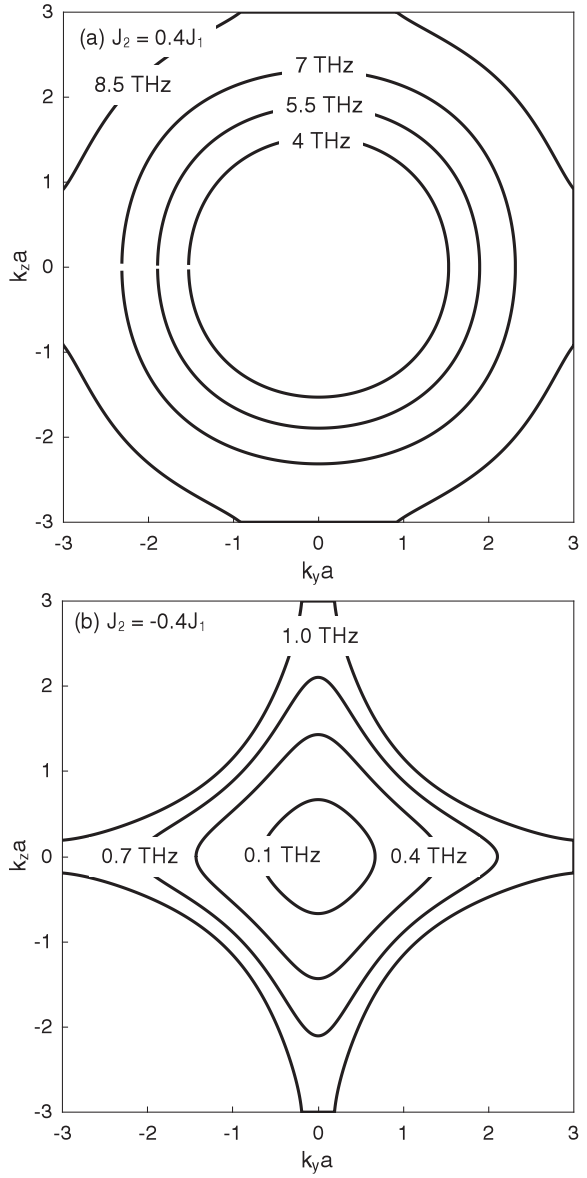

FIG. 4. Comparison of slowness surfaces for (a) $J_2 = 0.4J_1$ and (b) $J_2 = -0.4J_1$, with no fields. For positive next nearest neighbor interactions (a) the slowness surface is rounded and the next nearest neighbor contribution provides a different focusing direction from that of nearest neighbor interactions. Little focusing is expected. For negative next nearest neighbor interactions (b) an interesting pattern appears in the higher frequency cases (0.4 THz to 0.9 THz). There are two changes in curvature on each side of the focusing pattern.

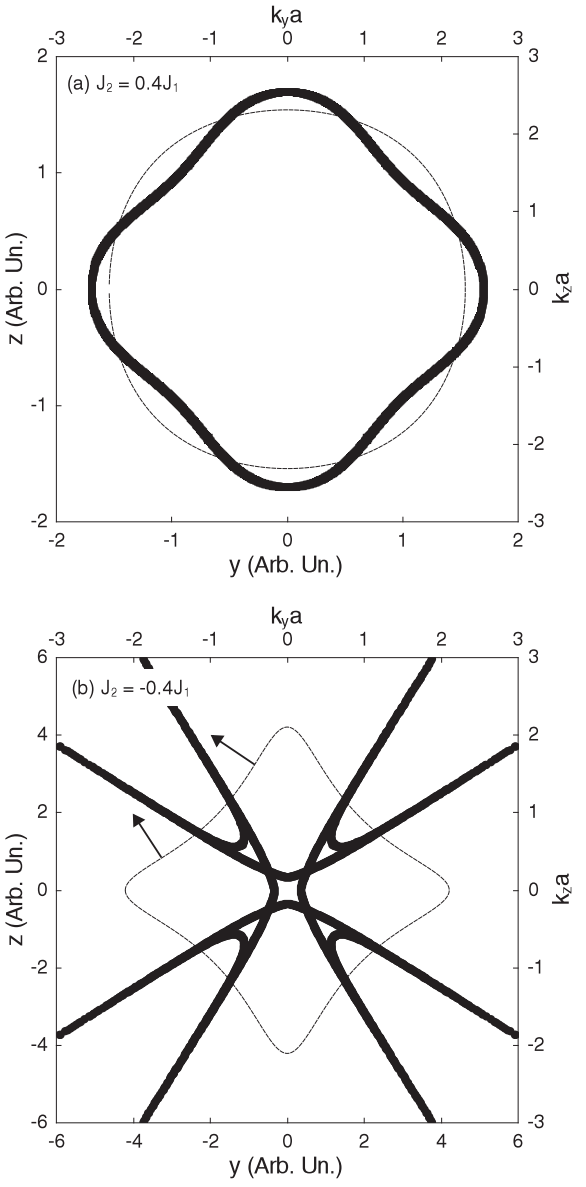

FIG. 5. Focusing patterns (dark curves using bottom and left axes) and associated slowness surfaces (light curves using top and right axis) for (a) $J_2 = 0.4J_1$ at $f = 7$ THz and (b) $J_2 = -0.4J_1$ at $f = 0.7$ THz, with no fields. For strong positive next nearest neighbor interactions (a) there is almost no focusing that occurs even at high frequencies. Note the focusing directions are different than in the case of nearest neighbor exchange interactions only. However, for strong negative next nearest neighbor exchange interactions (b) there is strong focusing at very low values of f. The arrows indicate two points on the slowness surface where the curvature is zero, giving caustics. There are now extra focusing directions (eight) compared to the four directions for nearest neighbor exchange only interactions.

slope at three neighboring points is calculated on the slowness surface. The change in slope between those three points gives the curvature at the middle point. Thus the focusing pattern is obtained by finding the vector normal to the slowness surface at a point, and the amplitude is given by the inverse of the square root of the curvature. Plotting the resulting amplitudes along the angle of the normal at each point produces a focusing pattern.

III. RESULTS AND DISCUSSION

For our calculations we use parameters similar to those of YIG, although we use the simplified spatial structure (square lattice) discussed earlier. The experimentally determined frequency of spin wave modes at the edge of the Brillouin zone (using $k_y a = \pi$ and $k_z = 0$ as the edge of the Brillouin

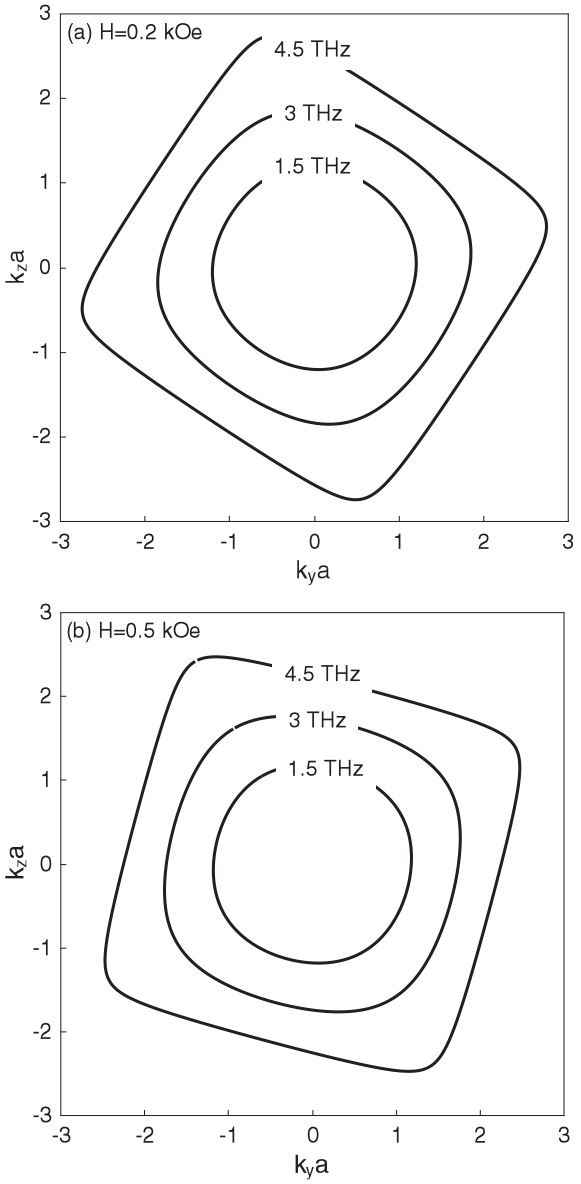

FIG. 6. Slowness surfaces for $\frac{K}{m} = -1$ kOe with (a) $H = 0.2$ kOe and (b) $H = 0.5$ kOe (right). Nearest neighbor interactions with an internal anisotropy field, and external H field perpendicular to anisotropy. Changing the field rotates the slowness surface, but the focusing still occurs between 4 and 5 THz as in the nearest neighbor only situation.

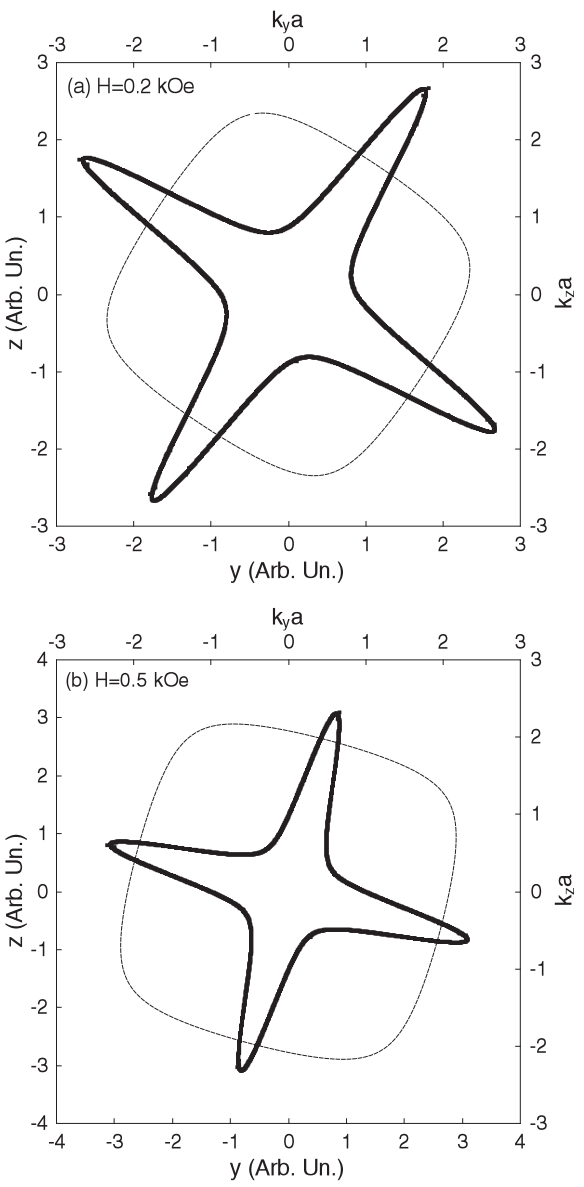

FIG. 7. Focusing patterns (dark curves using bottom and left axes) and the corresponding slowness surfaces (light curves using top and right axes) for $\frac{K}{m} = -1$ kOe (a) with $H = 0.2$ kOe and (b) $H = 0.5$ kOe (right) at $f = 4$ THz. The rotation of the focusing pattern demonstrates the tunability of the system. Notice the change in values of the axes.

zone) is at 7 THz [18]; this gives us $Jm = 400$ kOe and we take $\gamma = 0.0029 \frac{\text{THz}}{\text{kOe}}$.

Slowness surfaces and focusing patterns for the simplest case, nearest neighbor exchange only and no external magnetic field, are presented in Fig. 2 and Fig. 3. Near k=0, $\omega \approx Dk^2$, where D is the exchange constant. This leads to an isotropic slowness surface, i.e., a circle, in reciprocal k space resulting in no focusing at longer wavelengths. As k increases, the wavelength becomes shorter and closer to the lattice constant, and the wave "sees" the microscopic structure which introduces some anisotropy into the results. The constant frequency curves become squarelike for values of k about halfway through the Brillouin zone.

The change in the character of the slowness surface leads to a strong frequency-dependent focusing. For the lower frequency case of $f = 3$ THz, shown in Fig. 3(a), only weak focusing occurs. Strong focusing occurs when the curvature is near zero. In Fig. 3(b) and Fig. 3(c) we show focusing patterns for $f = 4$ THz and $f = 4.5$ THz that exhibit strong focusing.

The slowness surfaces and focusing plots for the case with both nearest and next nearest neighbor interactions are shown in Fig. 4 and Fig. 5. As with the nearest neighbor interactions shown in Fig. 3, only exchange interactions are considered, and no external fields. We considered J_2 with both the same sign and the opposite sign as J_1. For weak next nearest neighbor interactions the slowness surfaces do not change significantly

from that of nearest neighbor interactions. In contrast, Fig. 4(a) shows the slowness surface for large, positive, J_2. The slowness surfaces are rounded even for large frequencies; this would lead us to expect very weak focusing as is seen in Fig. 5(a).

When J_2 is negative and J_1 is positive the slowness surfaces [Fig. 4(b)] show an interesting feature. For frequencies between 0.4 THz and 0.9 THz the sides of the slowness surface have two changes in curvature. This is indicated in the specific case of $f = 0.7$ THz by arrows in Fig. 5(b). This leads to caustics caused by each change in curvature. Instead of four focusing directions as in Fig. 3, there are now eight directions of focusing. Furthermore, in this case the frequencies are shifted down significantly when compared to the nearest neighbor only interactions shown in Fig. 3. Strong focusing occurs around 0.1 THz compared to the 4.5 THz found with nearest neighbor only interactions.

For a single external field or internal anisotropic field, the character of the slowness surface from next nearest neighbor interactions is not changed significantly from that seen in the case of nearest neighbor exchange. The frequency values change with the strength of the field; however, the shape of the slowness surfaces remains the same.

In Fig. 6 and Fig. 7 we consider the case of an external magnetic field and magnetocrystalline anisotropy. With the H field in the z direction and a uniaxial anisotropy with the easy axis in the $\hat{y}$ direction, an equilibrium magnetization angle results. This equilibrium angle leads to a rotation (equal to the equilibrium angle) of both the slowness surfaces and the focusing patterns in the zy plane. By varying the field strength, the equilibrium angle and focusing direction change as seen in Fig. 6(a) and Fig. 6(b). This indicates system tunability and has potential as a spin-wave logic device [16]. Figure 7 shows that at certain values for f quite strong focusing remains, even when the slowness curve is rotated.

IV. SUMMARY

We examine the transmission of energy from a point source in a thin magnetic film and find that the energy spreads out uniformly for excitations with small wave vectors but is naturally focused into a small number of directions for excitations with larger wave vectors. This focusing does not require an external magnetic field, dipolar effects, or any magnetocrstalline anisotropy. Theoretical results were determined using the magnetic characteristics of YIG and show realistic values for the focusing frequencies. For the simple cubic model above, the strongest focusing occurs for frequencies between 4 and 5 THz.

We comment on the applicability of our calculation to real systems. YIG itself is not a simple cubic ferromagnet so it is unlikely to behave this way in reality. There are some simple cubic ferromagnets: NiCrPB, for example [19]. Surprisingly complex materials such as $La_{0.7}Pb_{0.3}MnO_3$ can also behave as simple cubic ferromagnets, and neutron scattering has verified the dispersion curves for this material over the entire Brillouin zone [20]. Although we derived focusing for a simple cubic ferromagnet, other cubic structures will give similar results. The relatively recent technique of spin-polarized electron energy loss spectroscopy can measure the entire spin-wave dispersion curve for very thin films, for example, an 8 monolayer thick Co film [21]. Furthermore, dispersion relations for high energy spin waves have been measured in body centered cubic Fe by neutron scattering [22].

Using the Landau-Lifshitz equations, the dispersion relations and the resultant focusing patterns were obtained for various cases. Constant frequency curves were plotted, and by evaluating the curvature of the slowness surfaces, focusing patterns were created. Strong focusing, i.e. caustics, occur when the curvature is zero. We find that the inclusion of next nearest neighbor exchange interactions can significantly change the nature and direction of the focused beams.

With an external magnetic field in the $\hat{z}$ direction and a uniaxial anisotropy with $\hat{y}$ as an easy axis, both in the plane of the lattice, the direction of the caustics can be adjusted by changing the magnetic field. The ability to control spin wave direction allows the development of signal processing systems. This could include, for example, demultiplexing of high frequency signals, where multiple signals of different frequencies could be incident on one antenna and then automatically separate into individual frequency beams within the magnetic material. Our results could also be important for spintronics, where the transfer of angular momentum is a key factor. We have shown the ability to strongly focus energy in particular directions which clearly also implies a focusing of angular momentum.

[1] Al. A. Kolomenskii and A. A. Maznev, Phys. Rev. B **48**, 14502 (1993).

[2] A. G. Every and W. Sachse, Phys. Rev. B **44**, 6689 (1991).

[3] G. A. Northrop and J. P. Wolfe, Phys. Rev. B **22**, 6196 (1980).

[4] B. Taylor, H. J. Maris, and C. Elbaum, Phys. Rev. Lett. **23**, 416 (1969).

[5] R. E. Camley and A. A. Maradudin, Phys. Rev. B **27**, 1959 (1983).

[6] J. C. Hensel and R. C. Dynes, Phys. Rev. Lett. **43**, 1033 (1979).

[7] Y. Tanaka, M. Narita, and S.-i. Tamura, J. Phys.: Condens. Matter **10**, 8787 (1998).

[8] C. S. Davies, A. V. Sadovnikov, S. V. Grishin, Yu. P. Sharaevskii, S. A. Nikitov, and V. V. Kruglyak, Appl. Phys. Lett. **107**, 162401 (2015).

[9] V. Veerakumar and R. E. Camley, Phys. Rev. B **74**, 214401 (2006).

[10] R. Gieniusz, H. Ulrichs, V. D. Bessonov, U. Guzowska, A. I. Stognii, and A. Maziewski, Appl. Phys. Lett. **102**, 102409 (2013).

[11] O. Büttner, M. Bauer, S. O. Demokritov, B. Hillebrands, Yu. S. Kivshar, V. Grimalsky, Yu. Rapoport, and A. N. Slavin, Phys. Rev. B **61**, 11576 (2000).

[12] T. Sebastian, T. Brächer, P. Pirro, A. A. Serga, B. Hillebrands, T. Kubota, H. Naganuma, M.

Oogane, and Y. Ando, Phys. Rev. Lett. **110**, 067201 (2013).

[13] M. P. Kostylev, A. A. Serga, and B. Hillebrands, Phys. Rev. Lett. **106**, 134101 (2011).

[14] T. Schneider, A. A. Serga, A. V. Chumak, C. W. Sandweg, S. Trudel, S. Wolff, M. P. Kostylev, V. S. Tiberkevich, A. N. Slavin, and B. Hillebrands, Phys. Rev. Lett. **104**, 197203 (2010).

[15] V. E. Demidov, S. O. Demokritov, D. Birt, B. O'Gorman, M. Tsoi, and X. Li, Phys. Rev. B **80**, 014429 (2009).

[16] K. Vogt, F. Y. Fradin, J. E. Pearson, T. Sebastian, S. D. Bader, B. Hillebrands, A. Hoffmann, and H. Schultheiss, Nat. Commun. **5**, 3727 (2014).

[17] C. Kittel, *Introduction to Solid State Physics*, 8th ed. (Wiley, New York, 2005), p. 333.

[18] A. V. Chumak, V. I. Vasyuchka, A. A. Serga, and B. Hillebrands, Nat. Phys. **11**, 453 (2015).

[19] D. M. Pajerowski, S. E. Conklin, J. Leão, L. W. Harriger, and D. Phelan, Phys. Rev. B **91**, 094104 (2015).

[20] T. G. Perring, G. Aeppli, S. M. Hayden, S. A. Carter, J. P. Remeika, and S.-W. Cheong, Phys. Rev. Lett. **77**, 711 (1996).

[21] R. Vollmer, M. Etzkorn, P. S. A. Kumar, H. Ibach, and J. Kirschner, Phys. Rev. Lett. **91**, 147201 (2003).

[22] A. T. Boothroyd, T. G. Perring, A. D. Taylor, D. McK. Paul, and H. A. Mook, J. Magn. Magn. Mater. **104-107**, 713 (1992).